2019-12

VERIFYING THE REPRESENTATION OF TROPICAL EASTERLY WAVES IN COMMUNITY CLIMATE MODEL VERSION 4

Davis, Wesley J.

Monterey, CA; Naval Postgraduate School

NAVAL POSTGRADUATE SCHOOL

MONTEREY, CALIFORNIA

THESIS

VERIFYING THE REPRESENTATION OF TROPICAL EASTERLY WAVES IN COMMUNITY CLIMATE MODEL VERSION 4

by

Wesley J. Davis

December 2019

Thesis Advisor: Joel W. Feldmeier
Co-Advisor: Scott Powell

THIS PAGE INTENTIONALLY LEFT BLANK

REPORT DOCUMENTATION PAGE			*Form Approved OMB No. 0704-0188*

1. AGENCY USE ONLY *(Leave blank)*	**2. REPORT DATE** December 2019	**3. REPORT TYPE AND DATES COVERED** Master's thesis

4. TITLE AND SUBTITLE VERIFYING THE REPRESENTATION OF TROPICAL EASTERLY WAVES IN COMMUNITY CLIMATE MODEL VERSION 4	**5. FUNDING NUMBERS**
6. AUTHOR(S) Wesley J. Davis	
7. PERFORMING ORGANIZATION NAME(S) AND ADDRESS(ES) Naval Postgraduate School Monterey, CA 93943-5000	**8. PERFORMING ORGANIZATION REPORT NUMBER**
9. SPONSORING / MONITORING AGENCY NAME(S) AND ADDRESS(ES) N/A	**10. SPONSORING / MONITORING AGENCY REPORT NUMBER**

11. SUPPLEMENTARY NOTES The views expressed in this thesis are those of the author and do not reflect the official policy or position of the Department of Defense or the U.S. Government.

12a. DISTRIBUTION / AVAILABILITY STATEMENT Approved for public release. Distribution is unlimited.	**12b. DISTRIBUTION CODE** A

13. ABSTRACT (maximum 200 words)

A descriptive evaluation of the Community Climate Model version 4 (CCSM4) was performed to assess its ability to realistically simulate African easterly wave (AEW) activity. Of particular interest, does a hindcast run of CCSM4 produce AEW at approximately the same frequency as documented in the Climate Forecasting System Reanalysis (CFSR) data set during the period 1979–2005? To address this, the meridional wind anomaly at 700 hPa was evaluated using an algorithm that employed a pattern of overlapping meridional means in an area bounded by 7°N to 15°N and 20°W to 25°W. This algorithm was designed to detect a meridional wind shift of 5 knots northerly to 5 knots southerly over a period of two days. The results indicate that CCSM4 simulates AEW at realistic frequencies as compared to CFSR. This method could be applied to the other variations of Climate Model Intercomparison Project 5 (CMIP5) to detect and evaluate AEW activity.

14. SUBJECT TERMS climate, reanalysis, model, modeling, CMIP, African easterly wave, wave, tropical easterly wave	**15. NUMBER OF PAGES** 43
	16. PRICE CODE

17. SECURITY CLASSIFICATION OF REPORT Unclassified	**18. SECURITY CLASSIFICATION OF THIS PAGE** Unclassified	**19. SECURITY CLASSIFICATION OF ABSTRACT** Unclassified	**20. LIMITATION OF ABSTRACT** UU

NSN 7540-01-280-5500

Standard Form 298 (Rev. 2-89)
Prescribed by ANSI Std. 239-18

THIS PAGE INTENTIONALLY LEFT BLANK

Approved for public release. Distribution is unlimited.

VERIFYING THE REPRESENTATION OF TROPICAL EASTERLY WAVES IN COMMUNITY CLIMATE MODEL VERSION 4

Wesley J. Davis
Lieutenant, United States Navy
BS, Devry University, 2002

Submitted in partial fulfillment of the
requirements for the degree of

MASTER OF SCIENCE IN METEOROLOGY AND PHYSICAL OCEANOGRAPHY

from the

NAVAL POSTGRADUATE SCHOOL
December 2019

Approved by: Joel W. Feldmeier
Advisor

Scott Powell
Co-Advisor

Wendell A. Nuss
Chair, Department of Meteorology

THIS PAGE INTENTIONALLY LEFT BLANK

ABSTRACT

A descriptive evaluation of the Community Climate Model version 4 (CCSM4) was performed to assess its ability to realistically simulate African easterly wave (AEW) activity. Of particular interest, does a hindcast run of CCSM4 produce AEW at approximately the same frequency as documented in the Climate Forecasting System Reanalysis (CFSR) data set during the period 1979–2005? To address this, the meridional wind anomaly at 700 hPa was evaluated using an algorithm that employed a pattern of overlapping meridional means in an area bounded by 7°N to 15°N and 20°W to 25°W. This algorithm was designed to detect a meridional wind shift of 5 knots northerly to 5 knots southerly over a period of two days. The results indicate that CCSM4 simulates AEW at realistic frequencies as compared to CFSR. This method could be applied to the other variations of Climate Model Intercomparison Project 5 (CMIP5) to detect and evaluate AEW activity.

THIS PAGE INTENTIONALLY LEFT BLANK

TABLE OF CONTENTS

THIS PAGE INTENTIONALLY LEFT BLANK

LIST OF FIGURES

THIS PAGE INTENTIONALLY LEFT BLANK

LIST OF TABLES

THIS PAGE INTENTIONALLY LEFT BLANK

LIST OF ACRONYMS AND ABBREVIATIONS

AEJ	African easterly jet
AEW	African easterly waves
CCSM4	Community Climate System Model version 4
CFSR	Climate Forecasting System Reanalysis
CMIP5	Coupled Model Intercomparison Project 5
hPa	hectopascals
JJAS	June, July, August, September
NCAR	National Center for Atmospheric Research
NOAA	National Oceanic and Atmospheric Administration
piControl	pre-industrial control
RCP	Representative Concentration Pathway

THIS PAGE INTENTIONALLY LEFT BLANK

ACKNOWLEDGMENTS

We acknowledge the World Climate Research Programme's Working Group on Coupled Modelling, which is responsible for CMIP, and we thank the National Center for Atmospheric Research for producing and making available their model output. For CMIP, the U.S. Department of Energy's Program for Climate Model Diagnosis and Intercomparison provides coordinating support and led development of software infrastructure in partnership with the Global Organization for Earth System Science Portals.

We would like to thank the following people for their valuable contributions: Dr. John Peters for his assistance in software development, Dr. Michael Montgomery, Dr. Tom Murphree, and Mr. Mark Boothe for their feedback on this experiment, Dr. Jeffrey Haferman and the NPS Hamming team for their technical expertise and data storage, and Mike Cook and Mary Jordan for their MATLAB expertise.

THIS PAGE INTENTIONALLY LEFT BLANK

I. INTRODUCTION

During the boreal summer, an intense temperature gradient between the Sahara Desert and Equatorial Africa creates a strong easterly flow known as the African Easterly Jet (AEJ) (Burpee 1972). Instabilities form to the north (south) of the AEJ and grow into African Easterly Waves (AEW) that propagate westward along approximately 20°N (10°N) (Reed and Hollingsworth 1988; Chen 2006; Pythouralis and Thorncroft 1995). AEW growth has been described as beginning with a large convective trigger over elevated terrain that subsequently grows though combined baroclinic/barotropic processes (Thorncroft et al. 2008). Once formed, these waves typically travel at a phase speed of 7–9 m s^{-1}, with periods of approximately 3–5 days (Burpee 1974; Reed et al. 1977). AEWs along the southern (10°N) track have been shown to be associated with tropical cyclone development in the Atlantic Ocean (Thorncroft and Hodges 2001; Chen 2006; Chen et al. 2008; Hopsch et al. 2007; Landsea 1993). Potential changes to AEW activity have been investigated using the outputs from the Coupled Model Intercomparison Project (CMIP, Martin and Thorncroft 2015; Ruti and Dell'Aquilla 2010; Daloz et al. 2012; Skinner and Diffenbaugh 2013).

Several techniques have been used in past studies to quantify and track AEW activity. Fink and Reiner (2013) used 700 hPa meridional winds averaged over 7ºN–13ºN to create Hovmöller (longitude vs. time) diagrams and manually interpreted AEW activity by identifying westward propagating northerly to southerly shifts in wind direction. Thorncroft and Hodges (2001), Hodges (2003) and Dieng et al. (2016) used automated tracking systems that focused on identifying and following vorticity centers. Martin and Thorncroft (2015) used Eddy Kinetic Energy (EKE) as a proxy for AEW activity when comparing CMIP models to reanalysis data. Diedhiou et al. (1999) used spectral analysis of meridional winds to examine how the dominant periods of AEW activity modulate rainfall.

The listed studies detect AEWs with varying uncertainty. This research aims to examine the accuracy of AEW activity in hindcast runs of a climate change model with a

detection methodology designed to better clarify the inherent uncertainty involved. An understanding of the representations of AEW activity within historical runs of climate change models, under known conditions, is important prior to examining future runs under varied climate change scenarios. Ultimately federal, state, and local authorities interested in planning, disaster relief, and emergency management have a critical interest in events with connections to AEW activity. The frequency and strength of AEWs may be different as modeled under different future climate scenarios. More confidence in such results is possible if the same climate models are shown to have reasonable depictions of historical AEWs.

The major objectives were to 1) develop an objective method for characterizing AEW activity from CFSR and CCSM4 wind fields, and 2) determine if CCSM4 AEW activity is consistent with CFSR AEW activity, and characterize the uncertainty associated with the technique being used. A grid point "screen" technique was used in this research to detect AEW activity and compare a CMIP model, the Community Climate System Model, version 4 (CCSM4) to CFSR for the months of June through September (JJAS) for 1979–2005. The datasets are detailed in Chapter II. The methods used to prepare and analyze the data using the grid point screen method are detailed in Chapter III. Examination of the results, including frequency of detection in both CCSM4 and CFSR, and comparisons between the two sets, is in Chapter IV. Chapter V discusses conclusions and future research.

II. DATA AND MODEL OUTPUT

This experiment assessed whether CCSM4 simulates AEW activity over the eastern Atlantic in a manner consistent with activity represented in CFSR. Meridional wind output at 700 hPa from CCSM4 and CFSR were compared at the same temporal resolution, with spatial resolutions of 0.9° latitude by 1.25° longitude and 0.5° by 0.5°, respectively. Wave activity in CFSR was also compared against satellite imagery to confirm that the patterns detected coincided with the presence of AEWs.

A. CMIP5

CMIP5 is a set of climate experiments conducted by modeling groups from around the world with the goal of furthering the collective understanding of climate change (Taylor et. al. 2012). The strategy of the experiment's organizers centered around two different modeling goals: performing near-term integrations simulating anywhere from 10 to 30 years of climate activity and performing long-term integrations over several hundred years (Hibbard et al. 2007). Of the many long-term integrations that were completed, two types apply to this paper: Pre-Industrial Control (piControl) and Historical, both of which were executed using CCSM4.

B. CCSM4

The CCSM4 was created by the National Center for Atmospheric Research (NCAR) as their submission to the CMIP5 (Gent et. al 2011). All data was available at https://www.earthsystemgrid.org in NetCDF format. Its piControl run is a multi-century long term integration meant to provide a reference point for climate change research. The run spans multiple centuries without significant changes (such as the Industrial Revolution) to any of the forcing mechanisms. Thus, it is able to reach a climatological equilibrium against which long-term changes related to modern human activity can be measured.

CCSM4 was also used to run 34 historical climate simulations from 1850–2005. These runs were subdivided into nine ensembles of three to six members each as well as

two other individual runs. The initial conditions for each of these models were based off of one of six initial conditions drawn from various years in the piControl run. They were then divided into runs that focused on a combination of changes to the following externally imposed forcing agents: solar, volcanic, greenhouse gases, sulfate aerosols (direct and indirect effects), ozone (tropospheric and stratospheric), land use change, sea salt, dust (mineral and otherwise), and carbon (black and organic). Most output parameters are available as monthly means; however, one run did provide daily averaged values, and the output from this run was used herein.

The CCSM4 version used in this paper is the historical run r6i1p1 from 1 January 1976–31 December 2005. The model has a grid-point spacing of 0.9° (latitude) by 1.25° (longitude) at 8 standard pressure levels and was initialized with conditions from year 953 in the piControl model. CMIP5 models use shared historical datasets (as shown in Figure 1), such as solar irradiation, greenhouse gas concentrations, and historical volcanic aerosol spikes for their atmospheric forcing (Lean et al. 1995; Lamarque et al. 2010; Ammann et al. 2010).

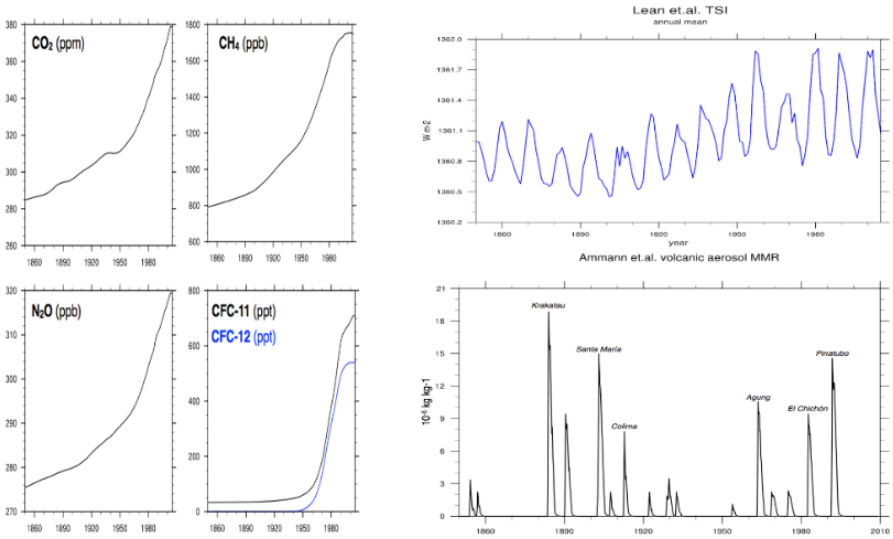

Left: Greenhouse gas concentrations from 1850–2005. Top right: Global mean solar irradiance. Bottom right: Volcanic aerosol emission events from 1850–2010. Charts drawn from: http://www.cesm.ucar.edu/CMIP5/forcing_information.

Figure 1. Examples of Atmospheric Forcing Used in CMIP5 Experiments.

C. CFSR

CFSR output was chosen as a proxy for observational truth for this experiment. CFSR is based off the Climate Forecasting System (CFS) model which was initialized four times daily (00 UTC, 06 UTC, 12 UTC, and 18 UTC) during the period 1979–2010. The spatial resolution of the CFSR data set for this experiment was 0.5 degrees and only the analysis fields were used. The analysis fields for each day were averaged together in order to make the temporal scale of CFSR consistent with CCSM4. The specific version of CFSR used is available at https://rda.ucar.edu/datasets/ds093.1/.

THIS PAGE INTENTIONALLY LEFT BLANK

III. METHODS

CCSM4 output was available as daily averaged values, so the first step was to take the 6-hourly CFSR data and construct CFSR daily averages. Then, an algorithm was developed that detected AEW passage in daily averaged CFSR and CCSM4, storing the dates of occurrence. Next, composites of all events in CFSR and CCSM4 were made for comparison and as a final quality control check before performing additional analysis of the data. Final analysis consisted of comparing the mean number of waves, wave period, and phase speed in each set of output.

A common technique for examining AEW activity using reanalysis data is to track the point at which the meridional wind is equal to zero, since it indicates a shift between northerly and southerly winds (e.g. Diedhiou et al. 1999; Kiladis 2006; Dieng and Sall 2016). This periodic wind shift is indicative of AEW passage. Since AEWs are cyclonic features, one must identify the points at which there is an abrupt change from northerly winds to southerly winds. The data for CFSR and the CCSM4 historical run overlapped for the years 1979–2005. Similar to Fink and Reiner (2013), in this experiment the meridional wind component at 700 hPa was examined. The region selected was over the Eastern Atlantic from 20°W–25°W and 7°N–15°N. This region was chosen because Diedhiou et al. (1999) indicated that the greatest concentration of AEWs coming off of Africa would be in this area. In order to isolate the AEW signal from the background noise, the seasonal cycle of the meridional wind at 700 hPa (v_{700}) was removed. Specifically, at each grid point, the mean value of v_{700} during 1979–2005 was separately computed for each day of four-month period being investigated and the resulting 122-day long time series at each grid point was considered to be the seasonal cycle.

Once this mean was removed, the AEWs were much easier to detect and track. In order offset the uncertainty associated with the magnitude, shape, and timing of AEW passage over the area being investigated, a grid point "screening" technique was developed to maximize the chances of detection. This technique consisted of detecting a prescribed change in meridional wind speed over 48 hours at five longitudes across the

region. For CFSR, these longitudes were 20°W, 21°W, 22.5°W, 24°W, and 25°W and for CCSM4 they were 20°W, 21.25°W, 22.5°W, 23.75°W, and 25°W. The region was also split into northern and southern latitude bands, centered around approximately 9.5°N and 12.5°N respectively, in order to increase the probability of detecting AEW passage. For this experiment, the northerly area was defined at 10ºN–15ºN and the southerly area was defined at 7ºN–12ºN. Because of the CCSM4 gridding, its output was examined from 7.05°N–12.72°N and 9.9°N–15.55°N.

Figure 2 shows the mean of the v_{700} seasonal cycle along with the two areas of detection and the grid points where AEW detection occurs. The northerly (southerly) areas are enclosed by dashed blue (red) boxes. The northerly (southerly) component is shaded blue (red), in 1 m s^{-1} intervals. The five longitudes checked by the algorithm are denoted in the center of the figure by faint vertically oriented gray lines, and longitudes near the coast of Africa and Brazil also similarly depicted. The latitudes inspected are listed on the ordinate. The northerly and southerly sections are outlined by blue and red dashed boxes, respectively. The two rows of grid points marked by X's centers of those sections and are the points at which AEW detection occurs. It is apparent in Figure 2 that CCSM4 does not accurately simulate the JJAS mean v_{700}, which ranges from 2 m s^{-1} over West Africa to 1 m s^{-1} between 20ºW and 25ºW while CFSR ranges from 4 m s^{-1} to 0 m s^{-1} over the same distance.

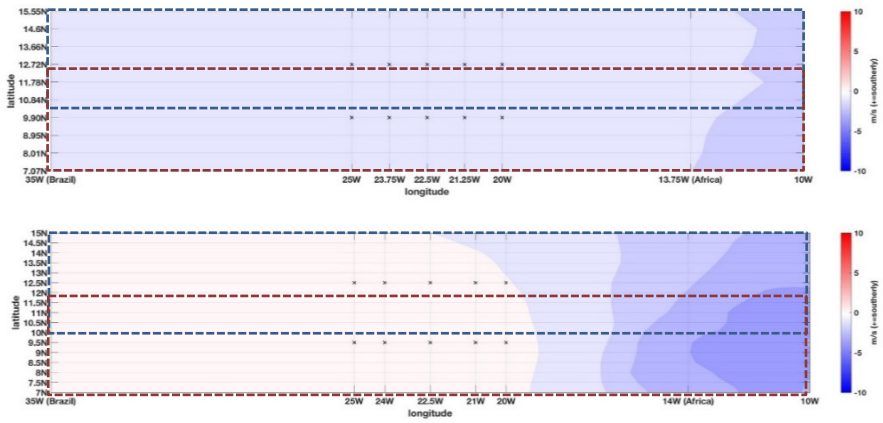

A comparison of CCSM4 (top) and CFSR (bottom) seasonal means of meridional component of winds in 1 meter per second intervals. Black X mark indicate grid points where AEW are to be detected. Blue and Red dashed boxes enclose northerly and southerly sections, respectively. CCSM4 area overlays are offset slightly in order to display grid points.

Figure 2. Seasonal Means for 1979–2005 with Grid Points Overlaid.

Next, an algorithm had to be created to detect AEWs. With the seasonal mean removed from the data only the anomalous values remained. These values were averaged over the northern and southern sections to come up with a mean *v* (meridional wind) anomaly for each section for every day. An AEW was considered to have been detected at a point if the mean *v* anomaly in the section being examined (northerly or southerly) changed from -2.6 m s^{-1} to +2.6 m s^{-1} over the course of two days. As a matter of quality control, the time steps at which wave passage was assumed to have occurred were compared with each other, and if two wave detections at a point were within 24 hours of each other, the first value was chosen and the other(s) discarded in order to prevent double counting. Figure 3 illustrates the process of translating meridional wind shifts of specific magnitudes into AEW detection. It demonstrates that AEWs of different speeds and magnitudes are detected differently, and also that not every wave is detected. This is expected, as the algorithm was designed to overlook AEWs with a wind shift below 5 knots (2.6 m s^{-1}), meaning that this study is focused on identification of the strongest easterly waves moving westward from Africa.

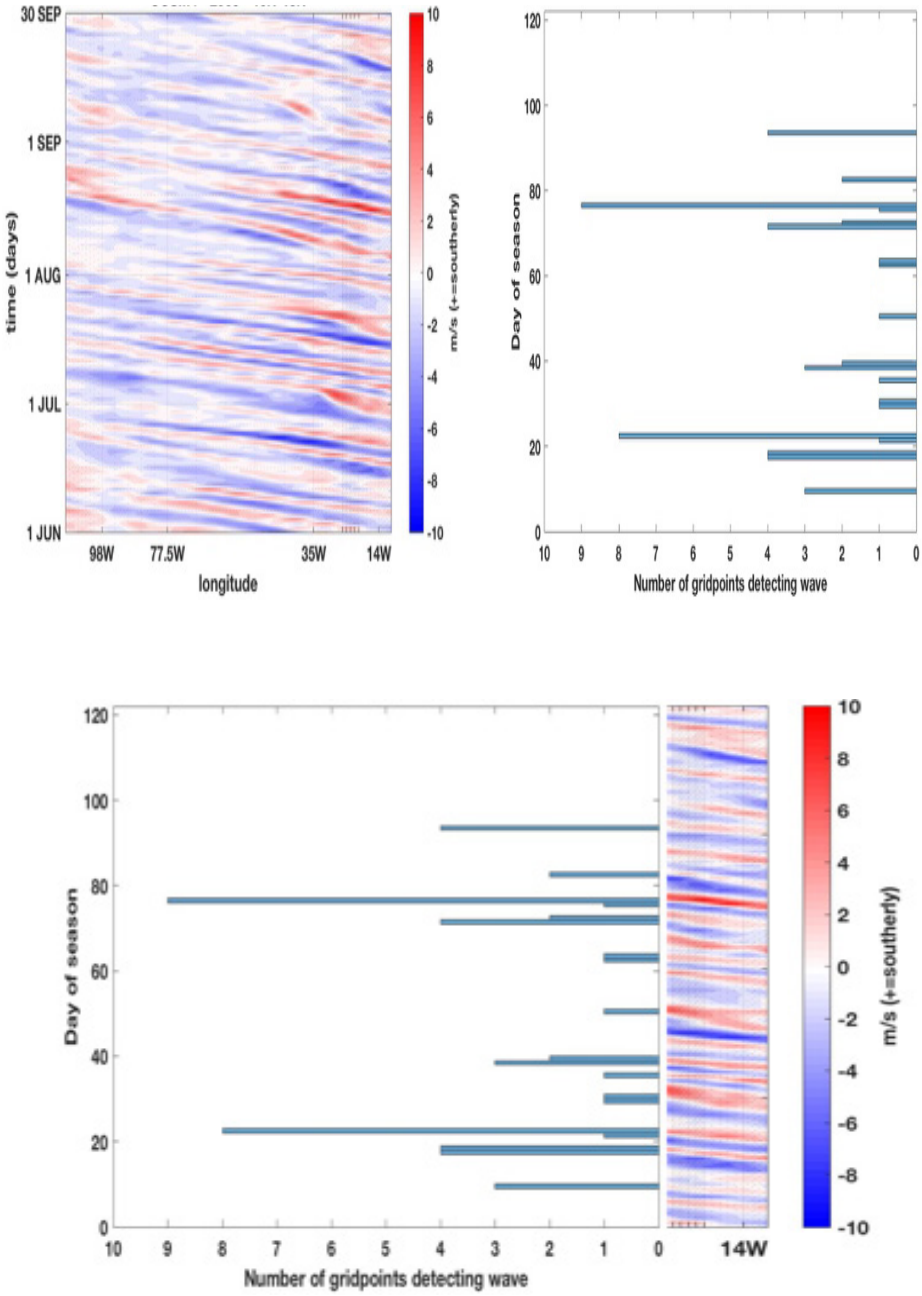

Top left: Hovmöller Diagram of mean meridional winds between 10°N and 15°N from 10°W to 110°W. Top right: Histogram of AEW detection from the grid point algorithm. Bottom: Combination of the two, with the histogram beginning from the western edge of the area being inspected (25°W).

Figure 3. Comparison of Meridional Winds and AEW Detection for JJAS 2005.

The approach adopted in this experiment was to divide the area into northerly and southerly sections, inspecting each independently in order to increase the probability of

detection. This improved overall detection sensitivity is on display in Figure 4 and clearly shows the sensitivity to AEW passage is more pronounced when the latitude range of the meridional mean is decreased. AEW were detected in the left image (southerly area mean) image that were not detected in the right image (entire area mean). Because the algorithm searched for a specific magnitude of wind shift, splitting the area into southern and northern portions prevented over-averaging that led to AEW signal dilution. Additionally, the decision was made to overlap the two areas across 10°N to 12°N, with the goal of making both areas more sensitive to AEW passing through the region. Dividing the area into two sections made the algorithm more likely to detect changes in the mean values of the two smaller sections than the mean value of the entire area. With the two areas defined, the next step was to define each area by its mean wind. In each dataset, the mean wind was defined for a given longitude as the mean across the latitudes in either the northern or southern area. These mean winds were plotted against time to highlight where a rapid change in the meridional wind would occur.

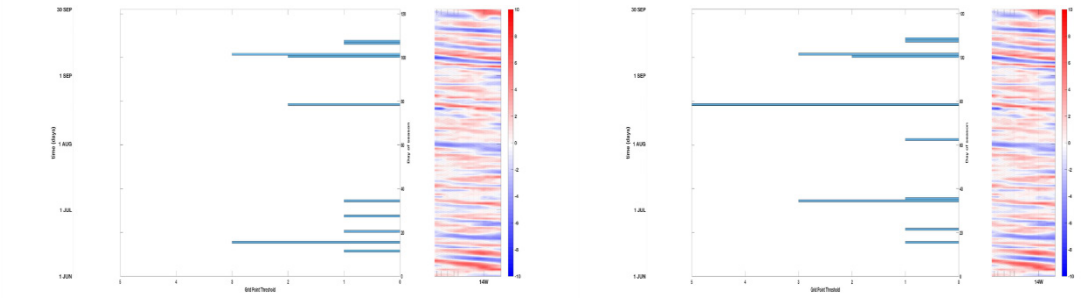

Left: Algorithm tuned to detect AEW passage using meridional winds from southern section of area. Right: Algorithm tuned to detect AEW passage using mean meridional winds across entire area. Background winds are the southerly section anomalous meridional mean winds from 2005.

Figure 4. Comparison of Detection Algorithms.

To confirm that the algorithm was operating properly, a composite analysis was performed. If every wind field at the time of detection of an AEW was averaged together, the result would depict northerly winds to the west and southerly winds to the east, with a sharply defined shift between them. This idea was tested by averaging the wind field at

the dates where AEWs were detected at 22.5°W for both data sets. Figure 5 shows the results of this composite analysis with CFSR on top and CCSM4 on bottom. Each image has northerly (southerly) winds shaded blue (red) in 1 m s^{-1} intervals. They both show a composite average of *v* anomalies during all detected AEW events at 22.5°W. Both images show northerly winds to the west and southerly winds to the east, consistent with the observed horizontal structure of AEWs (Kiladis et al. 2006) in both their shape and their v_{700} magnitudes. AEWs in CCSM4 seem to tilt into the cyclonic shear while in CFSR the tilt is more neutral. More investigation is needed in order to determine if this has implications on the energy transfer between AEW and the AEJ.

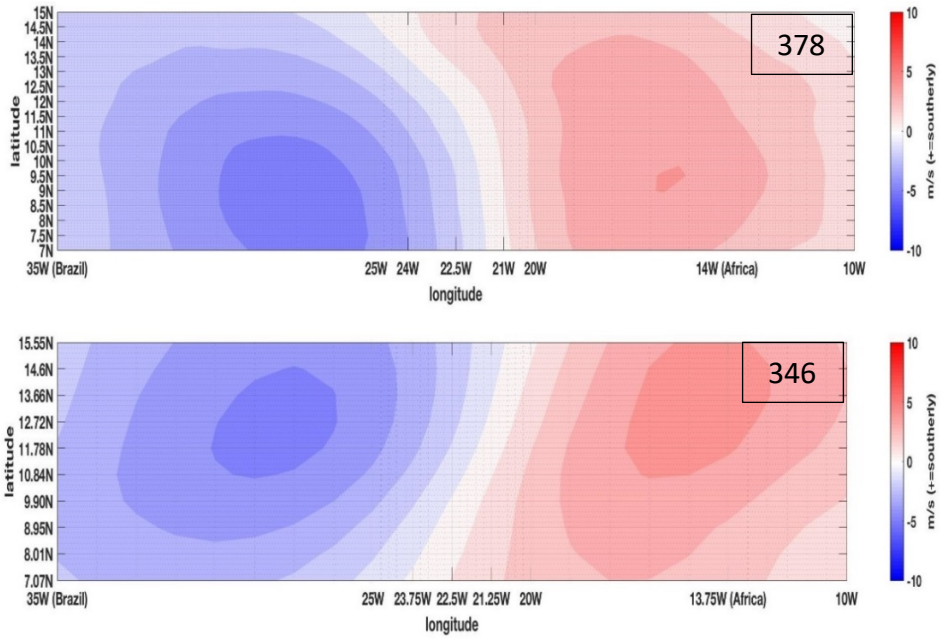

Average anomalous wind field for all times at which a TEW was detected at 22.5°W from 1979 to 2005. Contours are in 1 m/s intervals. Number of wind fields in each composite is displayed in bolded box at the top right of each image.

Figure 5. CFSR vs. CCSM4 Composite Analysis.

Phase speeds of the AEW in both data sets were sampled using manual inspection. A diagonal line that corresponded with 7.5 m s^{-1} (approximately 28° of longitude at 12°N over 5 days) was placed over the meridional wind shift as viewed in

Hovmöller diagrams. An example of this technique is on display in Figure 6, which shows these phase speed lines overlaid on top of a Hovmöller of the northerly region in CCSM4 for the year 2005 with detected AEW events plotted alongside.

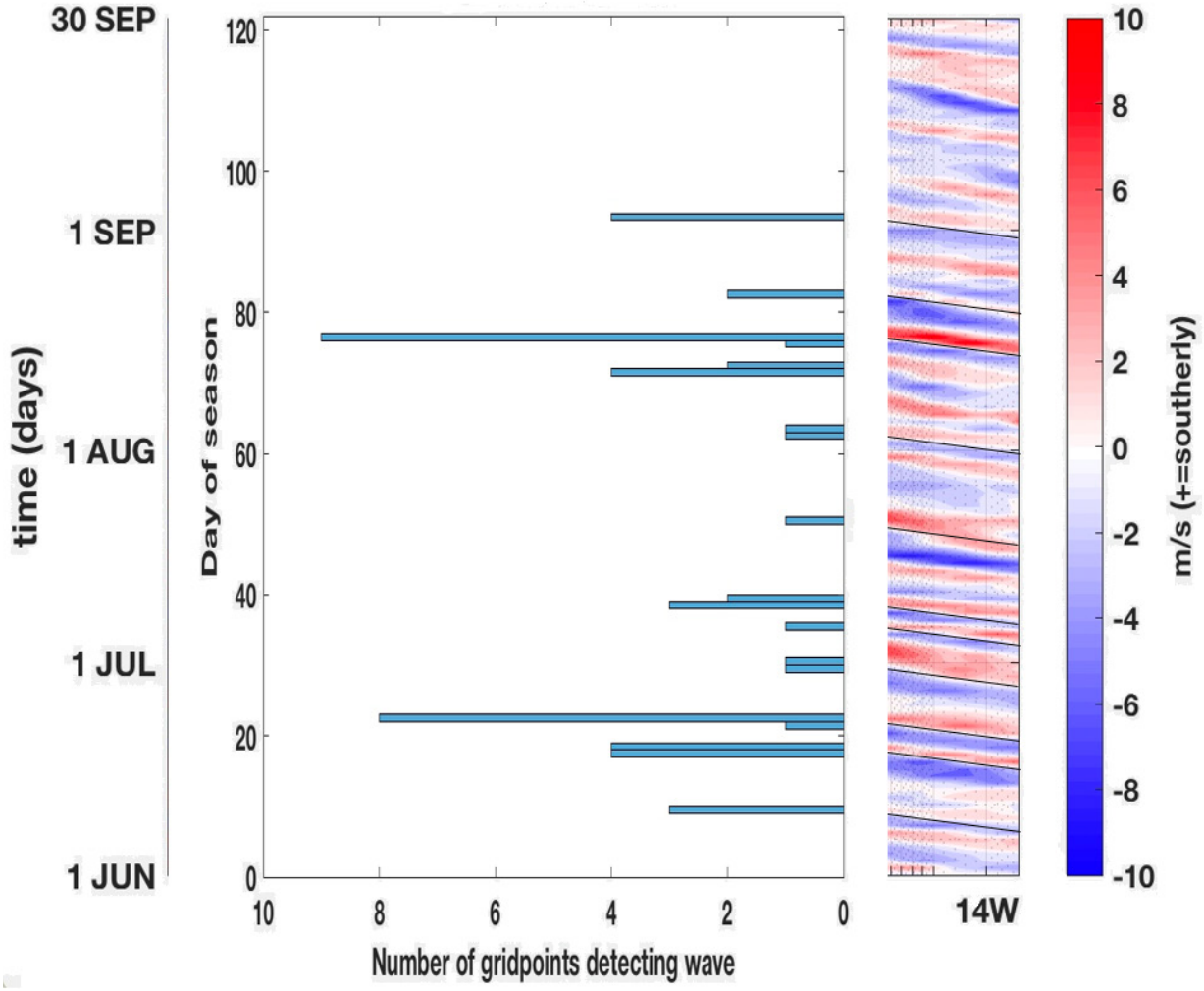

Right: Hovmöller diagram of CCSM4 meridional wind for JJAS of 2005 with phase speed lines overlaid in narrow black lines. Phase speed lines are calibrated to approximately 7.5 m s^{-1}. Northerly winds in blue, southerly in red. Left: Grid points detecting AEW events plotted over time for JJAS of 2005.

Figure 6. Phase Speed Check for CCSM4

THIS PAGE INTENTIONALLY LEFT BLANK

IV. RESULTS

At the end of each year's JJAS analysis, a mean interval between wave passage was calculated. Also, for each day in the time period, the number of grid points detecting a wave on that day were saved and used to create histograms. The number of instances was recorded for one grid point detecting wave passage, as well as two points detecting wave passage, and so on, up to all ten grid points (each denoted by an X in Figure 2) detecting a wave. These values were saved for each year and used to calculate the mean and standard deviation of the AEW seasonal occurrence over the entire period.

Twenty-seven seasons of data were analyzed in this experiment, with 122 days per season, giving a total of 3,294 possible days during which the algorithm could detect an AEW. For each day, how many grid points detected a wave were recorded. Figure 7 shows that, at first glance, both datasets have similar results. Inspection of Table 1 further reveals the degree of similarity, with each grid point threshold (exact number of the ten grid points detecting an AEW) within approximately 1% of each other.

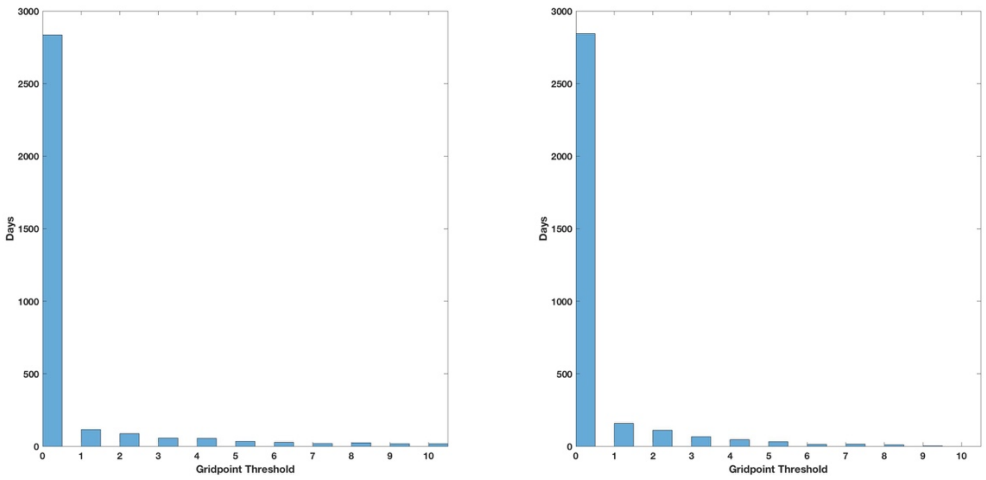

Histogram of AEW activity for CCSM4 (left) and CFSR (right). Each day in the total period was recorded as having detected an AEW at zero to ten points.

Figure 7. Total AEW Detections per Grid Point Threshold

Table 1. Total Wave Detections per Grid Point Threshold.

CCSM4	**Grid Points**	**0**	**1**	**2**	**3**	**4**	**5**	**6**	**7**	**8**	**9**	**10**
	Detections	**2836**	**116**	**88**	**58**	**54**	**34**	**28**	**21**	**24**	**17**	**18**
	Percentage	**86.10**	**3.52**	**2.67**	**1.76**	**1.64**	**1.03**	**0.85**	**0.64**	**0.73**	**0.52**	**0.57**
CFSR	**Grid Points**	**0**	**1**	**2**	**3**	**4**	**5**	**6**	**7**	**8**	**9**	**10**
	Detections	**2844**	**157**	**111**	**66**	**45**	**31**	**12**	**15**	**10**	**3**	**0**
	Percentage	**86.33**	**4.77**	**3.37**	**2.00**	**1.37**	**0.94**	**0.37**	**0.46**	**0.30**	**0.09**	**0.00**

The interval between waves was recorded for each year and those values were used to calculate the mean interval between wave detections over the entire period for each grid point threshold in both datasets. From those values, the box plot in Figure 8 was produced. Figure 8 shows two data sets whose box plots overlap for all thresholds except for all ten grid points detecting a wave, which did not occur at all in the CFSR data set. Therefore, CCSM4 represents the frequency of AEW occurrence consistently with that in CFSR.

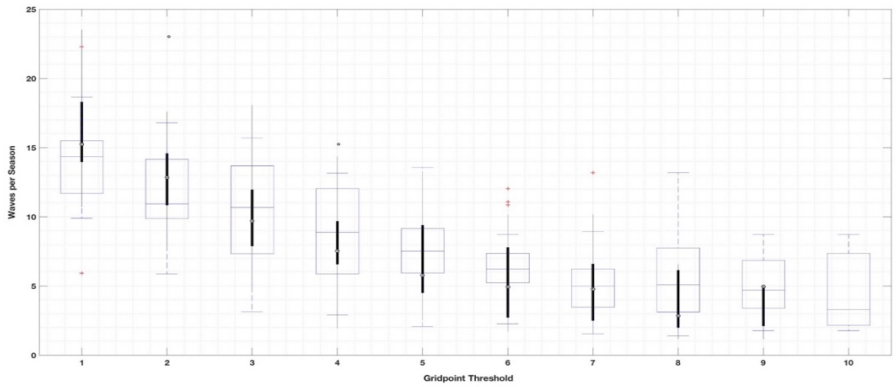

Box and Whisker plot of CCSM4 and CFSR. CCSM4 boxes are open and show first and third quartiles as their edges with a blue horizontal line for the median and blue horizontal lines at the ends of the whiskers for the min and max values. CFSR boxes are black and filled in. The median is an open circle with a black dot in the middle. The first and third quartiles are the edges of the thicker part and the min and max values are at the ends of the thin black lines protruding from the ends of the black boxes.

Figure 8. Box and Whisker Plots for Number of Waves per Season

V. DISCUSSION AND CONCLUSION

This experiment explored whether CCSM4 produced AEWs at the same climatological rate as shown in CFSR. In order to determine this, an objective method for identification of AEW in the region of interest had to be developed. The uncertainty associated with this method also had to be characterized in order to examine the data.

A raw count of AEW over the period seemed to be the most objective way to measure this phenomenon. The method described in this paper was developed with three guiding principles. First, was controlling for as many variables as possible. Hence the choice of using v_{700} just off of the coast of West Africa. The v_{700} wind shift is widely accepted as a valid method of detecting AEW. The area of interest controlled for orographic effects by being over the ocean and ocean effects by looking at AEW in a place where ocean modification would be at a minimum.

The second guiding principle was to collect the most accurate count possible, which led to development of the grid point method. Dividing the region into two section and looking for AEW at five points in each section minimized the chance that fluctuations in AEW as they passed through the area would prevent the algorithm from detecting their presence.

The final guiding principle was clarification of uncertainty. No method of AEW detection is perfect. All have their flaws and this method is no different. This method however gives an indication of the probability of accurate detection based upon how many points detected a wave on any one day or whether multiple detections were made over consecutive days.

The final analysis shows an overlap of results for both sets of output; therefore, we conclude that the CCSM4 historical run simulated the frequency of AEWs with a magnitude in 700 hPa meridional wind of at least 2.6m s^{-1} (5 knots) in a realistic fashion. Since the atmospheric forcing in this simulation was based off of actual historical data, this is an encouraging result. CCSM4-produced AEWs under future climate scenarios may provide useful context for those trying to assess climate change impacts.

A more in-depth analysis would examine all six available CCSM4 historical runs with the same atmospheric forcing and assess a range of responses. After that, an examination of historical runs with varied atmospheric forcing would provide some insight into what changes in the atmosphere would have the most significant effect on this phenomenon.

The AEWs detected by this algorithm fit a very specific mold. A specific magnitude of wind shift must occur at the prescribed location in order to be detected by this method. Any modification of these parameters would surely affect the final numbers. For instance, it is possible that increasing the v_{700} detection threshold above 5 kts would show that CCSM4 does not produce results that are comparable with CFSR.

Often, AEW signals are investigated using techniques that concentrate on 2–6 day bandpass filtered streamlines or some other manner of spectral analysis. This technique only searches for a specific magnitude of wind shift over two days. Exactly how results from these two techniques would overlap is unknown and may warrant further research.

This study reveals that narrowing down the range where meridional averages are taken provides useful information. Often, researchers average over the entire northern or southern AEW track (Thorncroft and Hodges, 2001; Martin and Thorncroft, 2015). This research showed that by taking averages over smaller areas, it was possible to detect AEWs that would have been missed otherwise.

It might also be possible to correlate patterns of grid point detections to AEW size and development cycles. Future research could focus on expanding this grid point technique to 850 hPa and 925 hPa vorticity as well as 700 hPa meridional winds. These values could be averaged across overlapping latitudinal increments of 5° from 15°N to 7°N for example. An animation of these detections overlaid across a map of North Africa might reveal a condensed view of the life cycle of an AEW and provide researchers a way to specifically zero in on a particular event based on how they are detected using this method.

Another possible use of this technique would be to correlate AEW detections based off this method to precipitation distribution. For example, Skinner and Diffenbaugh

(2013) compared the 2–6 day bandpass filtered v_{700} variance and mean precipitation in a suite of CMIP3 models to ERA-Interim reanalysis combined with Global Precipitation Climatology Project data. The bandpass filtered meridional wind does not distinguish between westerly and easterly patterns. It also does not reveal anything about frequency, intensity, or timing of AEW events. Using this method would provide a way to account for all of that, while also being able to correlate location and magnitude of specific AEW events to precipitation locations and magnitudes.

THIS PAGE INTENTIONALLY LEFT BLANK

LIST OF REFERENCES

Ammann, C. and P. Naveau, 2010, Mar.: A statistical volcanic forcing scenario generator for climate simulations," *J. Geophys. Res*. *Atmos*, **115**, D05.

Burpee, R.W., 1972: The origin and structure of easterly waves in the lower troposphere of North Africa. *J. Atmos. Sci*., **29**, 77–90, https://doi.org/10.1175/1520-0469(1972)029<0077:TOASOE>2.0.CO;2

Burpee, R.W., 1974: Characteristics of North African Easterly waves during the summers of 1968 and 1969. *J. Atmos. Sci*., **31**, 1556–1570, https://doi.org/10.1175/1520-0469(1974)031<1556:CONAEW>2.0.CO;2

Chen, T., 2006: Characteristics of African easterly waves depicted by ECMWF reanalyses for 1991–2000. *Mon. Wea. Rev*., **134**, 3539–3566, https://doi.org/ 10.1175/MWR3259.1

Chen, T., S. Wang, and A.J. Clark, 2008: North Atlantic hurricanes contributed by African easterly waves north and south of the African easterly jet. *J. Climate*, **21**, 6767–6776, https://doi.org/10.1175/2008JCLI2523.1

Daloz, A. S., F. Chauvin, K. Walsh, S. Lavender, D. Abbs, and F. Roux, 2012: The ability of general circulation models to simulate tropical cyclones and their precursors over the North Atlantic main development region. *Climate Dynamics*. **39**, 1559–1576, http://dx.doi.org.libproxy.nps.edu/10.1007/s00382-012-1290-7

Dee D.P. et al., 2014: Toward a consistent reanalysis of the climate system. *Bull. Amer. Meteor. Soc*., **95**, 1235–1248.

Diedhiou, A., S. Janicot, A. Viltard et al., 1999: Easterly wave regimes and associated convection over West Africa and tropical Atlantic: results from the NCEP/NCAR and ECMWF reanalyses. *Climate Dynamics*, **15(11)**, 795–822. https://doi.org/ 10.1007/s003820050316

Dieng, A.L., S.M. Sall, L. Eymard, M. Leduc-Leballeur, and A. Lazar, 2017: Trains of African easterly waves and their relationship to tropical cyclone genesis in the Eastern Atlantic. *Mon. Wea. Rev*., **145**, 599–616, https://doi.org/10.1175/MWR-D-15-0277.1

Fink, A. H. and A. Reiner, 2003: Spatiotemporal variability of the relation between African easterly waves and West African squall lines in 1998 and 1999. *J. Geophys. Res. Atmos*., **108**, D11, https://doi.org/10.1029/2002JD002816

Gent, P.R., G. Danabasoglu, L.J. Donner, M.M. Holland, E.C. Hunke, S.R. Jayne, D.M. Lawrence, R.B. Neale, P.J. Rasch, M. Vertenstein, P.H. Worley, Z. Yang, and M. Zhang, 2011: The Community Climate System Model Version 4. *J. Climate*, **24**, 4973–4991, https://doi.org/10.1175/2011JCLI4083.1

Hibbard, K. A., G. A. Meehl, P. M. Cox and P. Friedlingstein, 2007: A strategy for climate change stabilization experiments, Eos Trans. *AGU*, **88(20)**, 217– 221, doi:10.1029/2007EO200002.

Hodges, K., B. Hoskins, J. Boyle, and C. Thorncroft, 2003: A comparison of recent reanalysis datasets using objective feature tracking: storm tracks and tropical easterly waves. *Mon. Wea. Rev*, **131(9)**, 2012–2037. https://doi.org/10.1175/1520-0493(2003)131(0585:ACPSDF)2.0.CO;2

Hopsch, S.B., C.D. Thorncroft, K. Hodges, and A. Aiyyer, 2007: West African storm tracks and their relationship to Atlantic tropical cyclones. *J. Climate*, **20**, 2468–2483, https://doi.org/10.1175/JCLI4139.1

Kiladis, G. N., C. D. Thorncroft, and N. M. J. Hall, 2006: Three-dimensional structure and dynamics of African easterly waves. Part I: Observations. *J. Atmos. Sci*., **63**, 2212–2230.

Lamarque, J.F., T.C. Bond, V. Eyring, C. Granier, A. Heil, Z. Klimont , D. Lee, C. Liousse, A. Mieville, B. Owen, M.G. Schultz, D. Shindell, S.J. Smith, E. Stehfest, J. Van Aardenne, O.R. Cooper, M. Kainuma, N. Mahowald, J.R. McConnell, V. Naik, K. Riahi, D.P. Van Vuuren, 2010. Historical (1850-2000) gridded anthropogenic and biomass burning emissions of reactive gases and aerosols: Methodology and application. *Atmospheric Chemistry and Physics Discussions,* **10**, 4963–5019.

Landsea, C.W., 1993: A climatology of intense (or major) Atlantic hurricanes. *Mon. Wea. Rev*., **121**, 1703–1713, https://doi.org/10.1175/1520-0493(1993)121<1703:ACOIMA>2.0.CO;2

Lean, J., J. Beer and R. Bradley, Reconstruction of solar irradiance since 1610: Implications for climate change, *Geophys. Res. Lett*., **22**, 3195-3198, 1995.

Martin, E.R. and C. Thorncroft, 2015: Representation of African easterly waves in CMIP5 Models. *J. Climate*, **28**, 7702–7715, https://doi.org/10.1175/JCLI-D-15-0145.1

Martin, E.R. and C. Thorncroft, 2015: Representation of African easterly waves in CMIP5 models. *J. Climate*, **28**, 7702–7715, https://doi.org/10.1175/JCLI-D-15-0145.1

Pytharoulis, I. and C. Thorncroft, 1999: The low-level structure of African easterly waves in 1995. *Mon. Wea. Rev*., **127**, 2266–2280, https://doi.org/10.1175/1520-0493(1999)127<2266:TLLSOA>2.0.CO;2

Reed, R., E. Klinker, A. Hollingsworth, 1988: The structure and characteristics of African easterly wave disturbances as determined from the ECMWF operational analysis/forecast system. *Meteorology and Atmospheric Physics*, **38**,1-2, 22–33, https://doi-org.libproxy.nps.edu/10.1007/BF01029944.

Ruti, P. and A. Dell'Aquilla, 2010: The twentieth century African easterly waves in reanalysis systems and IPCC simulations, from intra-seasonal to inter-annual variability. *Climate Dynamics*, **35**, 1099–1117, https://doi.org/10.1007/s00382-010-0894-z

Saha, S., and Coauthors, 2010: NCEP climate forecast system reanalysis (CFSR) selected hourly time-series products, January 1979 to December 2010. research data archive at the National Center for Atmospheric Research, computational and information systems laboratory, Boulder, CO. [Available online at https://doi.org/10.5065/D6513W89.] Accessed† 02 Oct 2019.

Skinner, C. B., and N. S. Diffenbaugh, 2013: The contribution of African easterly waves to monsoon precipitation in the CMIP3 ensemble, *J. Geophys. Res*. *Atmos*., **118**, 3590– 3609, doi:10.1002/jgrd.50363.

Taylor, K.E., R.J. Stouffer, and G.A. Meehl, 2012: An overview of CMIP5 and the experiment design. *Bull. Amer. Meteor. Soc*., **93**, 485–498, https://doi.org/10.1175/BAMS-D-11-00094.1

Thorncroft, C. and K. Hodges, 2001: African easterly wave variability and its relationship to Atlantic tropical cyclone activity. *J. Climate*, **14**, 1166–1179, https://doi.org/10.1175/1520-0442(2001)014<1166:AEWVAI>2.0.CO;2

Thorncroft, C.D., N.M. Hall, and G.N. Kiladis, 2008: Three-Dimensional Structure and Dynamics of African Easterly Waves. Part III: Genesis. *J. Atmos. Sci*., **65**, 3596–3607, https://doi.org/10.1175/2008JAS2575.1

THIS PAGE INTENTIONALLY LEFT BLANK

INITIAL DISTRIBUTION LIST

1. Defense Technical Information Center
   Ft. Belvoir, Virginia

2. Dudley Knox Library
   Naval Postgraduate School
   Monterey, California